Measurement of atomic-hydrogen spin-exchange parameters at 0.5 K using a cryogenic hydrogen maser

M. E. Hayden,* M. D. Hürlimann,† and W. N. Hardy
Department of Physics, University of British Columbia, Vancouver, British Columbia, Canada V6T 1Z1
(Received 29 September 1995)

Using a cryogenic hydrogen maser, suitably modified to have electronic control of both the resonance frequency and the quality factor of the external cavity, we have measured a number of spin-exchange parameters for an atomic-hydrogen (H) gas at a temperature of 0.5 K. These results are relevant to the ultimate achievable frequency stability for cryogenic H masers and, when coupled with accurate calculations of the spin-exchange parameters, serve as a sensitive test of the H-H interatomic potentials. We find evidence for a frequency shift not predicted by semiclassical theories of spin exchange. In the context of a fully quantum mechanical hydrogen-atom spin-exchange theory [B. J. Verhaar *et al.*, Phys. Rev. A **35**, 3825 (1987) and J. M. V. A. Koelman *et al.*, Phys. Rev. A **38**, 3535 (1988)], this frequency shift is attributed to the influence of hyperfine interactions during spin-exchange collisions. Our findings are generally in agreement with these predictions; however, the sign of the hyperfine-induced frequency shift appears to differ from theory.

PACS number(s): 34.90.+q, 06.30.Ft, 84.40.Ik, 67.65.+z

I. INTRODUCTION

One of the technological benefits resulting from efforts during the early 1980's to achieve Bose-Einstein condensation in atomic hydrogen was the ability to store and manipulate gases of these atoms at temperatures below 1 K. In particular, it became possible to conceive of operating hydrogen masers, the most stable of all frequency sources for intermediate averaging times, at very low temperatures. The advantages of low-temperature operation, which include weaker collisional broadening, lower thermal noise, and less sensitivity to thermal perturbations, were first discussed by Vessot *et al.* [1] and Crampton *et al.* [2]. Detailed analyses of potential frequency stability were given by Hardy and Morrow [3] and Berlinsky and Hardy [4]. Estimates of fractional frequency stabilities as high as one part in 10^{18} over periods of 1 h were derived, representing a thousandfold improvement over existing masers.

In rapid succession, three groups observed maser oscillations below 1 K [5–7] using van der Waals films of superfluid liquid ^{4}He (l-^{4}He) as wall coatings. The University of British Columbia (UBC) cryogenic hydrogen maser (CHM) exhibited a stability greater than that of the best conventional H masers over short (1–3 sec) averaging times [8,9], in reasonable agreement with expectations.[1] Unlike conventional H masers which are based on an atomic beam apparatus [10], the UBC CHM is a recirculating device in which the hydrogen atoms are continuously circulated between the maser cavity and a microwave pumped state inverter [11]. The inherently cryogenic nature of this maser offers many advantages over conventional designs.

At about the same time, Verhaar and several of his collaborators presented a fully quantum mechanical treatment of the hydrogen-atom spin-exchange problem and calculated the relevant parameters over a wide range of temperatures [12–14]. Their results indicated that at low temperatures, both the frequency shifts and line broadening caused by collisions between H atoms are more complicated functions of the hyperfine level populations than at room temperature. They investigated the implications of their calculations for the operation of cryogenic H masers and concluded that the conventional method [15] used to suppress the influence of atomic density fluctuations on the maser oscillation frequency f would not be nearly as effective at low temperatures. In the absence of an alternative scheme for decoupling f from its dependence on the atomic density, this implied that earlier estimates of potential frequency stability were likely not achievable.

In this article we describe our investigations of H-atom spin-exchange collisions at 0.5 K using a modified version of the UBC CHM. Specifically, we have undertaken an experiment designed to examine the behavior of the oscillation frequency of the maser as a function of the tuning and quality factor of the external resonator, as well as the atomic density within the storage bulb. Analysis of the data in terms of the fully quantum mechanical H-atom spin-exchange theory allows us to extract a number of frequency shift and broadening cross sections relevant to the ultimate achievable frequency stability of cryogenic H masers. When coupled with accurate calculations of the spin-exchange parameters, the data should also prove to be a sensitive test of the H-H interatomic potentials.

We begin, in Sec. II, with a review of spin-exchange collisions and the influence they have on the operation of a hydrogen maser. This is followed in Sec. III by a description

*Present address: Department of Condensed Matter and Thermal Physics, MS K764, Los Alamos National Laboratory, Los Alamos, NM 87545.

†Present address: Schlumberger-Doll Research, Old Quarry Road, Ridgefield, CT 06877.

[1]Meaningful stability measurements over longer averaging times were not possible due to the lack of suitable reference sources available to the UBC group.

of the experimental apparatus with emphasis on modifications made to the UBC CHM for the purpose of this work. In Sec. IV we outline our experimental procedures and then in Sec. V our data is analyzed in terms of the spin-exchange theory of Verhaar and collaborators. The implications of this work are discussed in Sec. VI.

II. SPIN-EXCHANGE AND CAVITY PULLING

In a dilute gas of paramagnetic atoms, interatomic collisions cause the hyperfine levels to shift and broaden or, more generally, add terms to the evolution of the single-atom density matrix. These so-called spin-exchange effects play a central role in the details of the operation and stability of the hydrogen maser. During the 1960s a number of authors treated these collisional effects in a degenerate internal states (DIS) approximation, which ignores hyperfine interactions during collisions [15–18]. In this approximation, the frequency shift of the $\Delta F=1$, $\Delta m_F=0$ hyperfine transition is exactly proportional to the overall rate of collisions (and therefore to the atom density) and to the difference between the relative populations of the $m_F=0$ levels. Making use of the fact that pulling of the resonance by a detuning of the microwave cavity is proportional to the same factors, Crampton [15,18] showed that for a certain detuning the masing frequency became independent of the H density in the cavity. This procedure has since come to be known as spin-exchange tuning and is a critical step in the operation of any high-stability hydrogen maser.

Crampton and Wang reexamined this problem in 1975 [19], using a semiclassical approach to include hyperfine interactions during spin-exchange collisions. An additional frequency shift that is not suppressed by the usual spin-exchange tuning procedure was predicted. They obtained experimental evidence for such an effect using a conventional maser operating at room temperature. The magnitude of the shift, however, was small enough that it was of little practical importance.

With the advent of cryogenic H masers which are generally operated at much higher densities, and which potentially have greater intrinsic frequency stabilities, it became important to examine the issue more carefully. In two important papers Verhaar and co-workers [12,13] (hereafter referred to as VKSLC) presented the first fully quantum mechanical treatment of hydrogen-atom spin-exchange collisions. They also investigated in detail how an operating maser would be affected by instabilities in the atom collision rate, or equivalently, the H-atom density. Their calculations show that while none of the spin-exchange terms in the density matrix are actually larger at 0.5 K (the operating temperature of the UBC CHM) than at room temperature, the interplay between the various terms is such that spin-exchange tuning is less effective at cryogenic temperatures.

In low but finite magnetic field where coherences are only induced between the $|a\rangle$ and $|c\rangle$ hyperfine states[2] (see Fig. 1), the frequency shift and atomic linewidth of the $\Delta F=1$,

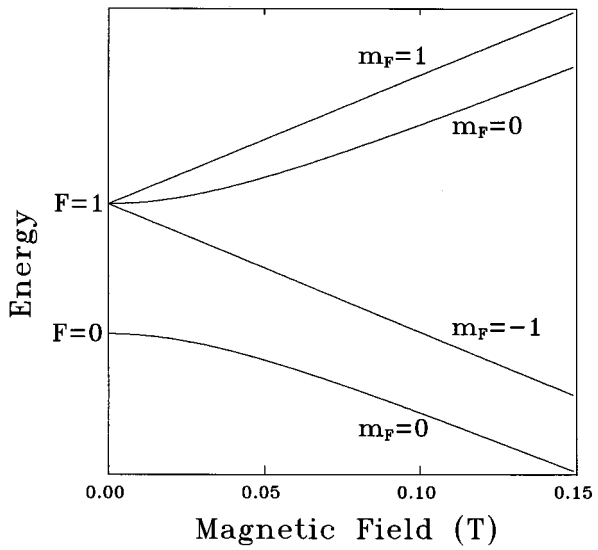

FIG. 1. Energies of the four hyperfine states of the ground electronic state of the hydrogen atom as a function of magnetic field. These states are labeled $|a\rangle$, $|b\rangle$, $|c\rangle$, and $|d\rangle$ in order of increasing energy in low magnetic fields. Atoms in the $|a\rangle$ and $|b\rangle$ states are drawn towards regions of high magnetic field and are referred to as *high field seekers*. Conversely, atoms in the $|c\rangle$ and $|d\rangle$ states are referred to as *low field seekers*. H masers are operated on the $|c\rangle$ to $|a\rangle$ or $\Delta F=1$, $\Delta m_F=0$ transition which near zero field occurs at $\omega_0/2\pi\cong 1420.405\,751$ MHz. The effective temperature of the zero-field splitting is $\hbar\omega_0/k_B\approx 68$ mK.

$\Delta m_F=0$ transition (i.e., the *a*-*c* transition) due to spin-exchange collisions are given in the VKSLC theory as

$$\omega-\omega_0=[\overline{\lambda_0}(\rho_{cc}-\rho_{aa})+\overline{\lambda_1}(\rho_{cc}+\rho_{aa})+\overline{\lambda_2}]\overline{v}n_{\mathrm{H}}, \quad (1)$$

$$\Gamma_c=[\overline{\sigma}_0(\rho_{cc}-\rho_{aa})+\overline{\sigma}_1(\rho_{cc}+\rho_{aa})+\overline{\sigma}_2]\overline{v}n_{\mathrm{H}}, \quad (2)$$

where the $\overline{\lambda_i}$ and $\overline{\sigma_i}$ are thermally averaged spin-exchange frequency shift and broadening cross sections, n_{H} is the atomic density, ρ is the 4×4 single-atom spin density matrix, and

$$\overline{v}=\sqrt{16k_BT/\pi m_{\mathrm{H}}} \quad (3)$$

is the mean relative velocity of the hydrogen atoms with mass m_{H}. In writing Eq. (1) we have denoted the density independent frequency by ω_0. In practice, this frequency will differ from the unperturbed atomic hyperfine transition frequency at the appropriate bias field by additional density-independent frequency shifts such as those caused by collisions of the H atoms with the storage bulb walls or with a buffer gas. Reference [13] gives theoretical values of $\overline{\lambda_i}$ and $\overline{\sigma_i}$ for temperatures ranging from 10^{-3} to 10^3 K. In Table I we list several values of the important products $\overline{\lambda_i}\overline{v}$ and $\overline{\sigma_i}\overline{v}$ at temperatures relevant to the operation of both conventional and cryogenic H masers [20].

In addition to the direct spin-exchange frequency shift represented by Eq. (1), the oscillation frequency of the maser is indirectly influenced by spin-exchange broadening [Eq.

[2]We have adopted the notation where the four hyperfine states of the electronic ground state of the H atom are labeled $|a\rangle$, $|b\rangle$, $|c\rangle$, and $|d\rangle$ in order of increasing energy in low magnetic field.

TABLE I. Calculated values [13,20] of the spin-exchange frequency shift parameters $\overline{\lambda_i}\overline{v}$ and broadening parameters $\overline{\sigma_i}\overline{v}$ in units of cm^3/s.

Parameter \ $T=$	0.5 K	300 K
$\overline{\lambda}_0\overline{v}$	-1.72×10^{-11}	-3.2×10^{-11}
$\overline{\lambda}_1\overline{v}$	-2.57×10^{-14}	1.3×10^{-13}
$\overline{\lambda}_2\overline{v}$	-1.67×10^{-14}	-2.4×10^{-13}
$\overline{\sigma}_0\overline{v}$	5.93×10^{-14}	-9.2×10^{-14}
$\overline{\sigma}_1\overline{v}$	7.59×10^{-13}	-2.1×10^{-11}
$\overline{\sigma}_2\overline{v}$	1.08×10^{-15}	4.3×10^{-10}

(2)] via the process of cavity pulling. An offset between the resonant frequency ω_c of the cavity and the oscillation frequency of the maser leads to a frequency shift that is proportional to the full[3] atomic linewidth Γ:

$$\omega-\omega_c=\Delta\Gamma, \tag{4}$$

where the cavity detuning Δ is defined by

$$\Delta\equiv Q_l\left(\frac{\omega_c}{\omega}-\frac{\omega}{\omega_c}\right)\approx 2Q_l\left(\frac{\omega_c-\omega}{\omega}\right) \tag{5}$$

and Q_l is the loaded quality factor of the maser cavity. A single expression describing the shift of the maser oscillation frequency caused by spin-exchange and cavity detuning effects can be obtained by first imposing the requirement that the oscillating magnetization **M** within the storage bulb be consistent with its own radiation field **H** within the resonator. This allows one to write the steady-state population inversion within the resonator as

$$(\rho_{cc}-\rho_{aa})n_{\mathrm{H}}=\frac{\beta}{\overline{v}}(1+\Delta^2)\Gamma, \tag{6}$$

where for convenience we have defined

$$\beta=\frac{4\overline{v}}{\mu_0\eta Q_l\hbar(\gamma_e+\gamma_p)^2}\ , \tag{7}$$

η being the effective ''filling factor'' for the storage bulb, and γ_e and γ_p the absolute values of the gyromagnetic ratios of the electron and proton, respectively. We then assume that the only density-dependent part of the linewidth is that due to spin-exchange collisions, i.e.,

$$\Gamma=\Gamma_0+\Gamma_c, \tag{8}$$

where Γ_c is given by Eq. (2) and all other contributions to the linewidth are contained in the term Γ_0. As a result of the dynamics of an oscillating maser, the difference $(\rho_{cc}-\rho_{aa})$ is much smaller than the sum $(\rho_{cc}+\rho_{aa})$. The broadening term in Eq. (2) proportional to $(\rho_{cc}-\rho_{aa})$ is thus very small and can be neglected. The full expression describing the combined spin-exchange/cavity pulling frequency shift of an oscillating H maser can therefore be written:

$$\begin{aligned}\omega-\omega_0=&[\Delta+\beta\overline{\lambda_0}(1+\Delta^2)]\Gamma_0\\&+\{[\Delta+\beta\overline{\lambda_0}(1+\Delta^2)][\overline{\sigma}_1(\rho_{cc}+\rho_{aa})+\overline{\sigma}_2]\\&+[\overline{\lambda_1}(\rho_{cc}+\rho_{aa})+\overline{\lambda_2}]\}\overline{v}n_{\mathrm{H}},\end{aligned} \tag{9}$$

or

$$\omega-\omega_0=[\Delta+\beta\overline{\lambda_0}(1+\Delta^2)]\Gamma-\Omega\Gamma_c, \tag{10}$$

where we have adopted the notation of VKSLC in defining the dimensionless hyperfine-induced (h-i) frequency shift parameter

$$\Omega=-\frac{\overline{\lambda_1}(\rho_{cc}+\rho_{aa})+\overline{\lambda_2}}{\overline{\sigma}_1(\rho_{cc}+\rho_{aa})+1\overline{\sigma}_2}\ . \tag{11}$$

The advantage to writing $\omega-\omega_0$ in this way is that one can clearly see the effects of including hyperfine interactions in the spin-exchange calculations: in the DIS approximation Ω is identically equal to zero[4] and therefore there exists a detuning

$$\Delta=\Delta'=-\beta\overline{\lambda_0}+O(\beta^3\overline{\lambda_0^3}) \tag{12}$$

which makes the oscillation frequency independent of the *full atomic linewidth* Γ, and which in fact sets the net spin-exchange/cavity pulling frequency shift to zero. This is the classical spin-exchange criterion derived by Crampton [15,18] and which has been used with great success in stabilizing H masers ever since [10]. The inclusion of hyperfine interactions during spin-exchange collisions[5] as discussed by VKSLC results in a nonzero Ω. At room temperature, however, the value of Ω is small [$\approx3\times10^{-4}$ with $(\rho_{cc}+\rho_{aa})=0.5$ [13]] and one finds that in practice it does not limit the frequency stability of conventional H masers. As the temperature of the H-atom gas is lowered, these effects can no longer be neglected. Intra-atomic hyperfine interactions fundamentally alter the rotational symmetry of the scattering problem by coupling the electronic and nuclear spins. The magnitude of Ω is expected to increase by a factor of about 250 as the temperature is lowered from 300 to 0.5 K. Under these conditions it is not possible to *completely* eliminate the density dependence of the maser oscillation frequency. Following Koelman *et al.* [13,14] one can define a modified spin-exchange tuning criterion

$$\Delta=\Delta''\approx-(\beta\overline{\lambda_0}-\Omega), \tag{13}$$

[3]i.e., Γ includes all sources of broadening.

[4]In the DIS approximation one finds $\overline{\lambda_1}=\overline{\lambda_2}=0$ and $\overline{\sigma}_0=0$, leaving $\overline{\lambda_0}$, $\overline{\sigma}_1$, and $\overline{\sigma}_2$ as the relevant parameters of the theory.

[5]The semiclassical theory developed by Crampton and Wang [19] predicted a nonzero value for $\overline{\lambda_2}$ in addition to the usual DIS terms.

where the oscillation frequency is made independent of the collision-dependent part of the linewidth Γ_c. This tuning leaves the maser frequency offset from ω_0 by $\Omega\Gamma_0$. Unfortunately Ω depends upon the sum $(\rho_{cc}+\rho_{aa})$, which in general depends upon the H-atom density and also on the strength of relaxation processes other than spin-exchange in a complicated way. Fluctuations in these parameters are thus coupled to the maser oscillation frequency. In addition, the frequency offset is directly affected by changes in the density-independent linewidth Γ_0.

III. TECHNICAL DETAILS

The design, operation, and performance of the UBC CHM have been described previously [6,8,9,11,21,22]. The most comprehensive review of the device is that found in Ref. [9]. Here, we only summarize a number of topics relevant to the present experiment.

A. Design and operation of the maser

In conventional hydrogen masers, a beam of atomic hydrogen is created and passed through a ''state-selecting'' region, typically the axis of a hexapolar magnetic field, such that only atoms in the two upper hyperfine levels ($|c\rangle$ and $|d\rangle$) are focused onto the entrance of a storage bulb situated within a low loss microwave cavity. This resonator is tuned to the a-c hyperfine transition frequency. When the density difference between the $|c\rangle$ and $|a\rangle$ states exceeds a certain threshold, stable maser action can be observed.

The fully cryogenic design of the UBC CHM differs radically from that of conventional masers, eliminating most problems associated with the introduction of an atomic beam into a cryogenic environment.[6] As described below, the UBC CHM is a recirculating device in which H atoms are first produced in a cryogenic source [24] and then continuously circulated between a state selection region (or ''state inverter'') where they are prepared in the upper hyperfine states, and the maser bulb, where they interact with the microwave cavity. Since the recombination lifetime of the atoms [25,26] at the operating temperatures and densities of the maser is very long, the atoms repeat this cycle many times before eventually reacting with other H atoms to form H_2.

The UBC CHM is housed within a commercial dilution refrigerator fitted with a custom designed, home-built, dilution unit [27]. It comprises several distinct interconnected volumes, all of which are coated internally with a saturated superfluid film of l-^{4}He. This film suppresses the adsorption of H atoms to the cold walls[7] and allows the maser to be operated at temperatures as low as 230 mK. From the standpoint of minimizing temperature-induced frequency fluctuations, the optimum operating temperature for the maser is of order 0.5 K. The exact temperature at which this occurs is geometry dependent; it is the temperature at which the combined frequency shift due to collisions between the H atoms and the liquid ^{4}He walls and that due to collisions with the ^{4}He vapor passes through a minimum [25].

H atoms are produced from solid molecular H_2 deposited on the walls of a low-temperature rf discharge source [24]. The rapid initiation of this discharge is facilitated by an internal ^{60}Co source of β particles. Normally the atom source is operated in a pulsed mode ($1\,\mu$sec duration, 0.4 W peak power, 0.1 s^{-1} repetition rate) to compensate for the slow decay of the H-atom density caused by recombination [25]. A large buffer volume (260 cm^3) was added prior to these experiments and acts to smooth out fluctuations in the atomic density caused by the pulsed discharge; it also reduces the area to volume ratio (A/V) of the maser and hence prolongs the recombination lifetime of the H atoms, which can be of order many hours at the lower densities.

A schematic diagram of the UBC CHM which illustrates the interconnection of various elements of the maser is shown in Fig. 2. The maser proper consists of a storage bulb and a state selector connected by a long ''atom'' tube. The storage bulb is located along the axis of a 1420-MHz split ring resonator (see Fig. 3) which in turn lies along the axis of a superconducting Pb shield. The Pb shield is used to trap a homogeneous longitudinal bias field of about 100 mGauss which not only sets a quantization axis for the H atoms but also suppresses cross relaxation between the upper three hyperfine states within the storage bulb. The split ring resonator [29] produces a longitudinal rf magnetic field which couples to the H-atom system [30,31]. It is used both as the microwave resonator for maser operation and as a means of interrogating the atomic gas with pulsed magnetic resonance techniques. The 5-cm^3 Pyrex glass storage bulb is located inside a thermalizing bath of superfluid l-^{4}He, which ensures a uniform temperature for the gas of H atoms. The atom tube and the storage bulb are connected via an orifice which sets the mean residency time of the atoms in the bulb. The state selector consists of a rectangular TM_{010} 40-GHz microwave cavity inside a 1.4-Tesla superconducting solenoid. The field is tuned such that the cavity can be used to pump either the $|a\rangle$ to $|d\rangle$ or the $|b\rangle$ to $|c\rangle$ ESR transition. Throughout the work we report here, the output frequency of the backward wave oscillator[8] (BWO) used to power the state selector was frequency stabilized to within a few tens of kHz using a quartz crystal oscillator. Variations in the output power level of the BWO were monitored and maintained at less than 1%.

[6]The principle advantage of this type of approach is related to the need for superfluid l-^{4}He wall coatings to reduce adsorption of H atoms to the inner walls of the maser. In order to bring a noncryogenic atomic beam into this environment, it is necessary to break the superfluid film at some point. The subsequent refluxing of ^{4}He vapor driven by thermal gradients can be the source of severe heat loads in a cryogenic environment [23]. Furthermore, it necessitates the use of high-capacity pumps to keep the ^{4}He vapor density low enough so as not to attenuate the atomic beam.

[7]The adsorption energy of the H atom to l-^{4}He is of order 1 K; the most accurate measurement of this energy was in fact made using the UBC CHM [9,11]. Note that unlike the H atom, the H_2 molecule can penetrate the l-^{4}He film and adsorb to the underlying substrate [28]. This self-cleansing mechanism eliminates the buildup of H_2 within the maser.

[8]Micro-Power model 221.

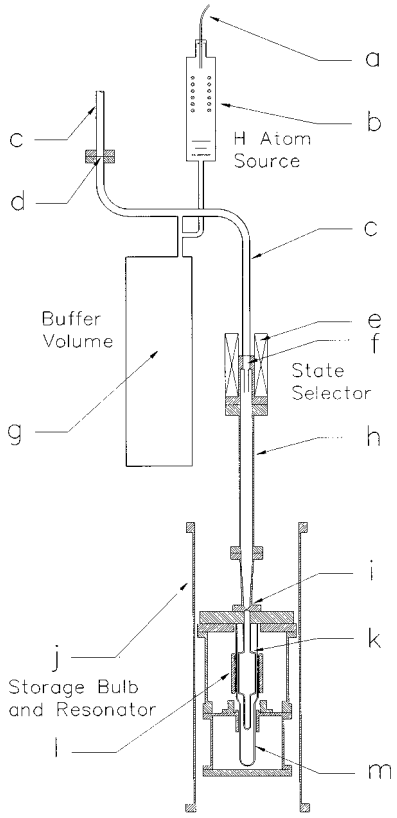

FIG. 2. Simplified schematic diagram which illustrates the interconnection of the principle low-temperature components of the maser as described in the text. Details include the (a) H_2 fill line, (b) H atom source, (c) waveguide for 40-GHz pump microwaves, (d) vacuum window, (e) 1.4-Tesla superconducting solenoid, (f) 40-GHz microwave cavity (atoms enter through a pin hole), (g) buffer volume, (h) ''atom'' tube, (i) orifice which sets the maser storage bulb holding time, (j) superconducting Pb shield, (k) inner (storage) bulb, (l) 1420-MHz maser resonator, and (m) outer (thermalizing) bulb which is filled with l-^{4}He. The scale of this figure is only approximate. A number of details such as the electronic tuning assembly shown in Fig. 4 have been omitted for the sake of clarity. See Figs. 3 and 4 as well as Refs. [9] and [11] for further details.

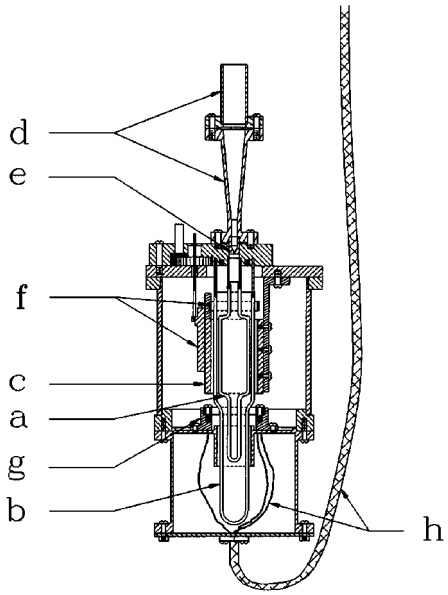

FIG. 3. Details of the UBC CHM 1420-MHz microwave resonator and storage bulb showing (a) the inner (storage) bulb, (b) outer (thermalizing) bulb which is filled with l-^{4}He, (c) 1420-MHz split-ring resonator, (d) atom tube leading to the state selector (see Fig. 2), (e) orifice, and (f) the mechanical tuning and coupling assembly (coaxial feed line not shown). Also indicated is the placement of (g) the electronic ''tuning ring'' which performs the dual functions of modifying the tuning and Q of the 1420-MHz resonator, and (h) the graphite bias leads for this assembly. The tuning ring is detailed in Fig. 4.

With the state selector turned off (no microwave pump), most of the high-field-seeking atoms ($|a\rangle$ and $|b\rangle$ states) reside in the state selector while most of the low-field-seeking atoms ($|c\rangle$ and $|d\rangle$ states) are located either in the storage bulb or in the atom tube. When microwave power is applied to the state selector, high-field-seeking atoms are converted to low-field seekers and are eventually expelled from the state selector. Cross relaxation induced by magnetic impurities near the entrance to the storage bulb ensures that the net flux of low-field seekers entering the storage bulb is distributed between the $|c\rangle$ and the $|d\rangle$ states. $|c\rangle$ state atoms are converted into $|a\rangle$ state atoms within the confines of the cavity via stimulated emission of radiation. Once low-field-seeking atoms leave the maser storage bulb they are drawn towards the state selector by the fringing fields of the 1.4-Tesla solenoid. Additional magnetic impurities embedded in a metallic foil and placed strategically near the entrance to the 40-GHz microwave cavity ensure that the flux of atoms entering the state selector are distributed between the $|a\rangle$ and the $|b\rangle$ states, thereby completing the cycle. The operating temperature of the state selector is maintained about 100 mK colder than that of the storage bulb. This improves the efficiency of the state selector by augmenting the magnetic compression factor; it also reduces the ^{4}He density in the atom tube and promotes faster circulation.

Once the net flux of $|c\rangle$ state atoms entering the storage bulb is sufficient to overcome dissipative losses associated with the microwave resonator, self-sustaining maser oscillations are obtained. The quality factor of the resonator is of order 10^3, with the result that the UBC CHM operates with H densities in the 10^{11} and 10^{12} cm^{-3} ranges. We note that this Q is intentionally lower than that of room-temperature masers so as to reduce cavity pulling effects.

The output of the maser (about 0.1 pW) is amplified by a GaAs FET preamplifier[9] operating at 4.2 K and then fed into a two-stage heterodyne detection system [24,33,9,22] at room temperature. The reference frequency for the detection system was derived from a high-quality quartz crystal oscillator[10] loosely phase locked to a Rb frequency standard[11] so as to improve its longterm stability. The frac-

[9]A home-built device, based on the design of Williams *et al.* [32].

[10]An Oscilloquartz ''very high stability'' OSA model 8600.03 BVA oscillator which was further temperature regulated using standard techniques.

[11]Efratom model FRK-L.

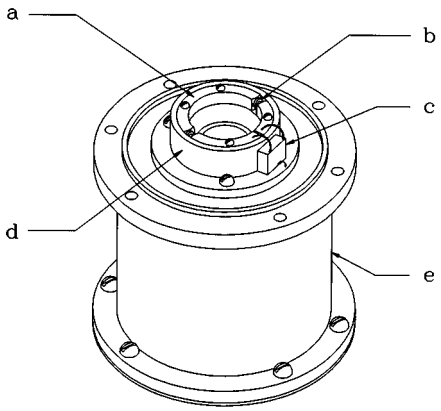

FIG. 4. The electronic ''tuning ring'' or ''Q spoiler'' shown mounted on the base of the Cu rf shield for the 1420-MHz resonator. The Cu structure (e) below this base simply acts as a housing for the graphite bias leads and as a thermal shield for the lower part of the maser storage bulb. Details indicated in this figure include (a) the Cu ring which comprises three partial annuli and is mounted to the (d) teflon support structure with nylon screws. The three gaps between the annuli are bridged by two varactor diodes (b), and a FET (c). Not shown are the graphite bias leads individually encased in Cu braid.

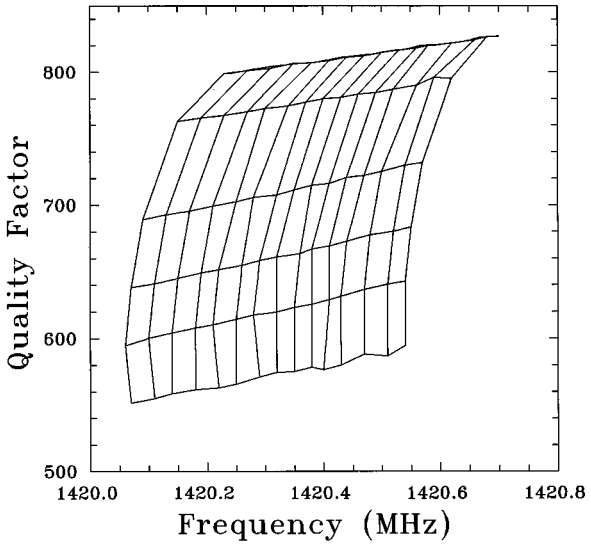

FIG. 5. A typical mapping of the resonant frequency and the quality factor of the 1420-MHz split-ring resonator as a function of the bias potentials applied to the varactor diodes (V_t) and the Q spoiling FET (V_q). ''Horizontal'' lines correspond to lines of constant V_q and ''vertical'' lines correspond to lines of constant V_t. Interpolation allows one to derive combinations of V_t and V_q which produce contours of constant tuning or constant Q.

tional frequency stability of the crystal oscillator is better than 5×10^{-13} for averaging times in the range 0.1–10 sec. The stability of the quartz-Rb combination is of order 1 part in 10^{12} over time periods comparable to the duration of the experiments, which limits our practical frequency resolution to about 1 mHz. The maser output is heterodyned down to a convenient (about 10 Hz) frequency, converted to a square wave by a limiting amplifier and then measured with an HP 5345 frequency counter. A direct measurement of the power output of the maser is made by injecting a calibrated signal into the section of coax between the maser and the preamplifier and thus measuring the gain of the detection system *in situ*. The heterodyne detection system can also be used as a 1420-MHz spectrometer for pulsed magnetic resonance experiments at the a-c transition.

B. "Tuning ring" or "Q spoiler" assembly

Both the tuning of the 1420-MHz split ring resonator and its coupling to the external circuitry can be varied by coarse mechanical adjustments. The primary modification to the UBC CHM for the purposes of studying the spin-exchange frequency shifts was the addition of a second resonator whose tuning and quality factor could be controlled by applying potentials to various semiconductor devices. Via the coupling between the two resonators, the tuning and the quality factor of the primary resonator can thus be changed in a highly controlled and reproducible manner.

The second resonator, which we alternately refer to as the ''tuning ring'' or ''Q spoiler,'' consists of a 2.5-cm diameter gold-plated Cu ring with a 3 mm by 3 mm square cross section (see Fig. 4). The ring is cut radially into three electrically isolated pieces to which various dc bias potentials are applied. GaAs varactor diodes[12] are mounted between two of the partial annuli while the third capacitive gap is filled with a 0.015-cm Teflon spacer. The latter gap is bridged electrically between the drain and the source of a GaAs FET[13] packaged in a hermetically sealed PLCC package.[14] Electrical contact to each section of the tuning ring and the gate of the FET was made using high-resistance graphite leads.[15] The various elements of the ring are held in place below the split ring resonator by a teflon former. Small metallic springs in series with the diodes and the ring accommodate motion caused by thermal contraction as the apparatus is cooled to sub-Kelvin temperatures.

The geometry of the tuning ring is such that its lowest resonance is close to 1900 MHz. By changing the bias potential V_t which is applied to the varactor diodes, the resonant frequency of the ring is shifted, in turn pulling the tuning of the 1420-MHz resonator. This geometry provided an effective tuning range of about 500 kHz or roughly 30% of the full width at half maximum (FWHM) of the 1420-MHz resonance. Similarly, by changing the bias potential V_q applied to the gate of the FET (essentially a variable resistance in the tuning ring), the Q of the tuning structure and hence

[12]Frequency Sources, Chelmsford MA 01824, model GC51105-57: these devices have a nominal capacitance of 0.6 pF with a bias potential of -4 V, and 1.6 pF at -15 V.

[13]NEC model 720: note that the prepackaged devices are sufficiently magnetic so as to warrant the effort of mounting dies in non-magnetic packages.

[14]Kyrocera America, Vancouver, WA 98661: part numbers PB45238 and KE77004-1.

[15]The Polymer Corporation, Reading, PA 19603.

that of the main resonator can be modified. This Q spoiler allowed us to vary the quality factor of the split-ring resonator between about 570 and 820 during the present experiments. Although the tuning and Q spoiling functions of the 1900-MHz ring are not completely independent of each other, by mapping out the resonant frequency and the Q of the split ring resonator as a function of the two bias potentials (see Fig. 5), a two-dimensional mapping can be constructed from which orthogonal changes in Q and Δ are easily derived.

IV. EXPERIMENTAL PROCEDURE

Ideally, a test of the spin-exchange-induced frequency shift described by Eq. (10) requires that the shift $\omega-\omega_0$ be measured while the 1420-MHz resonator frequency ω_c, its quality factor Q_l, and the densities $\rho_{ii}n_{\mathrm{H}}$ of all four hyperfine levels within the maser bulb are varied and monitored in a controlled manner. In addition, the filling factor η and the density-independent linewidth Γ_0 must be measured. By far the most difficult task in this overall strategy is the density measurement. In fact, during the current experiment, we did not have the ability to control or measure the four densities independently. Rather, we used magnetic resonance techniques to infer these densities somewhat indirectly. In the discussion which follows, we highlight our approach to the measurement of each of the parameters relevant to the investigation of spin-exchange frequency shifts in the UBC CHM.

A. Zero-field magnetic resonance: the free-induction decay

The combined spin-exchange–cavity-pulling frequency shift described by Eq. (10) is a function of the H-atom density in the storage bulb of the *oscillating* maser. This density cannot be measured directly and must be inferred from measurements of the atomic density made while maser oscillations are suppressed. The procedure we adopted for these measurements was to first stop maser action by attenuating the microwave power being fed into the state selector, and then to measure the atomic density in the storage bulb using pulsed magnetic resonance techniques [31]. While the maser is operating there is a constant flux of low-field-seeking atoms approaching the storage bulb. When the state selector is turned off, this flux is almost completely stopped. The H-atom density which is measured is thus less than that which is present inside the storage bulb of the oscillating maser.

We rely on a computer simulation of the quasi-steady-state dynamics of the maser to infer a ''density enhancement factor'' κ which relates the atomic densities in the nonoscillating maser to that in the oscillating maser [8,9]. This simulation has been used previously to model parameters such as the density dependence of the distribution of atoms between the four hyperfine states, and the power output of the maser. The results of the simulation depend upon factors such as the efficiency of the relaxing foil used to equalize the $|a\rangle$ and $|b\rangle$ state populations near the state selector. Reasonable assumptions for these parameters lead to a density enhancement factor of $\kappa=1.4$. Fortunately this value is only weakly dependent on the parameters of the model: we estimate that the uncertainty in κ is of order 5%. Note that we do not attempt to account for any variation of κ as the atomic density is changed. This model also predicts that the fraction of the atoms in the $m_F=0$ states inside the storage bulb is very close to 0.5 and that variations in the sum $(\rho_{cc}+\rho_{aa})$ are only about 4% over the full range of atomic densities for which the maser oscillates. In our analysis of the frequency shift data presented in the following section we implicitly assume that $(\rho_{cc}+\rho_{aa})$ remains constant.[16]

After suppression of maser action, the population distribution quickly approaches thermal equilibrium. Under these conditions and assuming weak coupling to the 1420-MHz resonator, the amplitude of a free induction decay (FID) response to a $\pi/2$ tipping pulse at the a-c hyperfine transition is proportional to the atomic density. The power emitted by the radiating atoms immediately following the rf pulse is given by

$$P=\frac{\mu_0\omega_0\hbar^2(\gamma_e+\gamma_p)^2V_b\eta Q_l}{8}\left[\frac{1-\exp\left(-\frac{\hbar\omega_0}{k_BT}\right)}{1+3\exp\left(-\frac{\hbar\omega_0}{k_BT}\right)}\right]^2 n_{\mathrm{H}}^2\,, \tag{14}$$

where V_b is the volume of the storage bulb and the other parameters are as described previously. Half of this power is transmitted to the detection circuitry when it is critically coupled to the resonator. By measuring this power, the atomic density can be determined.

An essential part of the density calibration procedure is the accurate measurement of the filling factor η. The filling factor for the storage bulb and resonator used in this work was measured using a perturbation technique that involves filling the maser storage bulb with liquid cryogens at temperatures just below 100 K [34]. When liquid O_2 (which is paramagnetic) is introduced to the storage bulb the frequency of the resonator is shifted because of the change in both the permeability and the permittivity relative to the empty cell. The dielectric contribution to this shift is accurately accounted for by subsequently filling the cell with liquid Ar, which has a relative permeability essentially that of free space and a dielectric constant very close to that of the liquid O_2. The residual paramagnetic contribution to the liquid O_2 frequency shift can then be related to the filling factor of the cell. Measured in this fashion the filling factor of the storage bulb and resonator used in this work was found to be 0.27(1). We note that prior to the introduction of the teflon support for the tuning ring, the filling factor for the storage bulb of the UBC CHM as measured in this way was 0.24(1).

The free induction decay response to a magnetic resonance tipping pulse contains considerably more information than just a measure of the atomic density. In particular, both the frequency and the initial phase of the FID are of considerable importance in the work described here. The frequency

[16]There is in fact no way to directly measure the distribution of atoms between the various hyperfine states given the present configuration of the UBC CHM.

of the FID is measured against the same oscillator used to measure the oscillation frequency of the maser. This provides a means to accurately determine the density-independent frequency ω_0, against which all frequency shifts are referenced.[17] The initial phase of the FID plays a less obvious but equally important role in the analysis of the data. An example of a FID response to a rf tipping pulse at the *a*-*c* hyperfine transition is shown in Fig. 6. Superimposed on the decay is a fit of the data to the relevant equations found in Appendix B of Ref. [31]. We note that the decay is not a simple damped exponential.

To elaborate on the role played by the initial phase of the FID one must consider the boundary conditions for reflection and transmission of rf signals to and from the 1420-MHz resonator. As the resonator is detuned from the local oscillator (LO) frequency, a fraction of the rf power which is injected as a magnetic resonance tipping pulse is reflected by the cavity. This introduces a phase shift between the LO and the rf field seen by the atoms. The magnitude of this effect is such that a detuning Δ increases the phase shift between the phase of the LO and the phase of the atomic coherence by an amount $\Theta=\Delta$. As the atoms precess and radiate power which is coupled back out of the detuned resonator, an additional phase shift $\Theta=\Delta$ is introduced between the atomic coherence and the detected FID response. The net result is that to first order, the initial phase of the detected FID is phase shifted by $\Theta=2\Delta$ with respect to the phase of the LO when the resonator is detuned by an amount Δ. Deviations from this linear phase relationship induced by higher order cavity pulling effects and spin-exchange frequency shifts can be neglected. The relevance of this relationship is that keeping track of the initial phase of a FID with respect to the LO as the resonator tuning is changed enables one to accurately measure the relative change in Δ *as seen by the atomic system*.

B. Resonator tuning and quality factor

Prior to carrying out the frequency-shift measurements, the resonance of the 1420-MHz split-ring resonator was tuned to the *a*-*c* hyperfine transition of the H atom and critically coupled to the external circuitry using coarse mechanical adjustments. The tuning and the quality factor of the resonator were then mapped out as a function of the bias potentials V_t and V_q applied to the semiconductor devices in the electronic tuning circuit. Δ and Q were determined by sweeping the frequency of an injected signal and fitting the reflected power to a single Lorentzian line shape with a linear background. An example of the grid of resonator tunings and quality factors so determined is shown in Fig. 5. A series of potentials enabling us to make orthogonal changes in Δ and Q were then derived from this data. During the present experiment, we restricted ourselves to two sets of parameters; a sequence of potentials giving rise to a series of detunings Δ at constant Q near the maximum obtainable Q, and a second sequence of Q's at a constant detuning near $\Delta=0$. We note that the reproducibility of a particular setting was better than the precision to which Q and Δ could be measured.

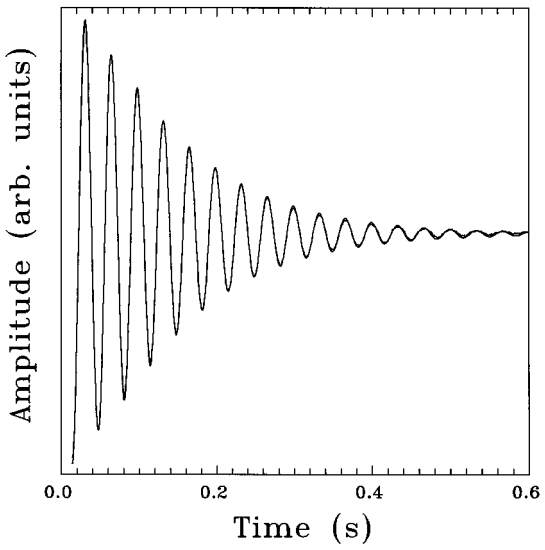

FIG. 6. An example of a FID response to a rf magnetic resonance tipping pulse at the *a*-*c* hyperfine transition of the H atom. A fit of the data to the relevant equations describing the decay [31] has been superimposed on the data. Note that the decay is not a simple damped exponential; roughly one quarter of the observed damping is caused by radiation damping [35]. This decay was recorded at 0.5 K with 7.1×10^{11} atoms per cm^3 in the maser storage bulb.

Reflection measurements of the tuning and the quality factor of the resonator are inherently susceptible to errors introduced by standing waves in the external circuitry. To estimate the influence of systematic errors introduced by these effects we measured the "*s*" parameters [36] of all components in the external circuitry, using an HP 8754A/H26 RF network analyzer, and used these as input to a commercial computer simulation of the microwave circuitry. Particular care was taken to investigate the effect of changes in the effective electrical length of coaxial cables both inside and outside of the dilution refrigerator.[18] The results of this analysis indicate that our measurements of quality factors should be accurate to about 1%. Discussion of the accuracy

[17]While in principal this procedure is straightforward, an *accurate* determination of the atomic frequency from the FID requires considerable care. Stimulated emission of radiation, which is responsible for maser action, also influences the free-induction decay. The coupling between the atomic system and the microwave field within the resonator causes the atoms to precess in their own radiation field. In this context, the effect is commonly referred to as radiation damping, and was studied in detail by Bloom [35]. Generalizations to general cavity tuning have been given by Morrow [33] and Hayden [22,31]. One finds that the effective precessing magnetization of the H atoms can be described by a set of differential equations which must be numerically integrated and fit to the FID data. Neglect of this effect can lead to the introduction of *apparent* frequency shifts in the analysis of FID data. All FID data reported here has been analyzed in this manner. A more thorough description of the actual analysis of this data can be found in Ref. [22].

[18]Induced, for example, by changing l-^{4}He levels in the 4.2-K bath of the dilution refrigerator.

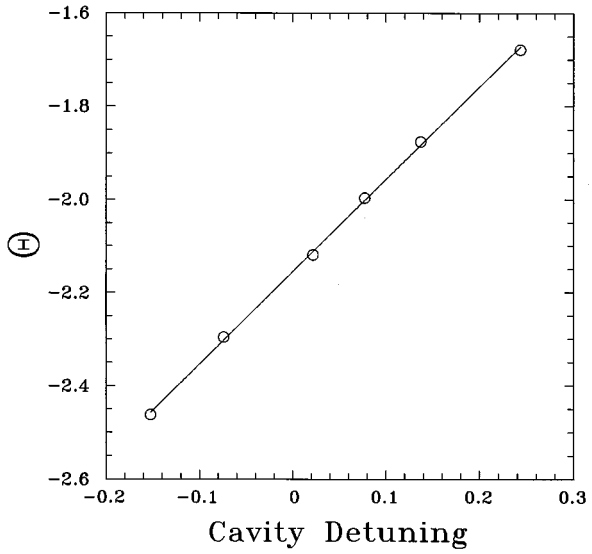

FIG. 7. The initial phase of the FID response as measured with respect to the phase of the local oscillator and plotted as a function of the measured resonator detuning, Δ. The slope of the line which has been fit to the data is 1.983(23) which is in agreement with the theoretical value of 2. From this result we infer that changes in the *relative* tuning of the resonator as measured in reflection are accurate to about 1%.

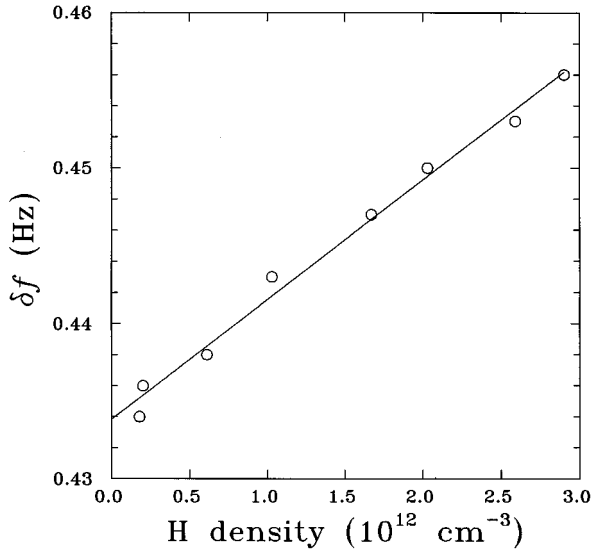

FIG. 8. The frequency of the FID response measured with respect to the frequency of the 1420.405...MHz local oscillator plotted as a function of the H-atom density within the maser storage bulb. The line fit to this data extrapolates to a zero density frequency of 1420.405 783 434(1) MHz which we take as the density independent transition frequency ω_0. Note that the uncertainty in this value is a measure of the precision and not the accuracy of the measurement. An arbitrary frequency of 1420.405 783 MHz has been subtracted from the data.

of the absolute cavity detuning is given in Sec. V.

It has previously been mentioned that relative detunings can be measured quite accurately by observing the initial phase of a FID as the tuning of the resonator is changed. In Fig. 7 the initial phase of a FID is plotted as a function of the resonator detuning determined by the reflection measurement described above. The theoretical slope of a line fit to this data should be 2. Experimentally we observe a slope of 1.983(23), from which we infer that our measurements of relative detunings are accurate to about 1%.

C. Frequency-shift measurements

Throughout the series of measurements described below, the H-atom density within the maser volume was maintained at a constant level by periodic firing of the rf discharge in the atom source. Changes in the density were made by varying the discharge pulse duration and repetition rate. Densities produced in this manner did not fluctuate measurably within the detection sensitivity, typically of order 1% the measured density.

Temperatures of the various volumes of the maser were measured using calibrated germanium resistance thermometers and regulated to within a few μK. The temperature of the storage bulb volume was maintained at a temperature of 0.500(3) K throughout the spin-exchange measurements. For the present experiments, the maser was operated in the mode where the $|a\rangle$-to-$|d\rangle$ ESR transition was pumped in the state selector.

Measurement of the maser output frequency has already been described; the power output of the maser was monitored using an HP 3478A ac voltmeter. Once stable maser operation was established at a given density, the frequency of the maser was measured several times in succession using a 10-sec averaging interval. This frequency measurement was then repeated as a function of the preset Q's and Δ's described above. At each setting the maser frequency was measured a minimum of three times. Multiple checks of the unperturbed oscillation frequency (maximum Q, $\Delta=0$) were made throughout these measurements. Maser action was then temporarily stopped by inserting a resistive card attenuator into the broad wall of the Ka band waveguide feeding the state selector.[19] This allowed the measurement of the H-atom density in the storage bulb of the maser with $\pi/2$ tipping pulses. The latter measurement was made in the unperturbed cavity setting. Maser action was then reestablished and the original operating conditions verified before moving on to the next series of measurements at a new H density. After repeating these measurements over a range of densities spanning the full operating range of the CHM, the Q and the detuning of the resonator at each of the preset conditions was remeasured.

V. ANALYSIS OF THE DATA

Some of the data obtained during the course of this work has previously been analyzed and reported [22,37,38]. We include this information here in attempt to present a comprehensive description of the data analysis.

[19]Rather than sweeping the microwave frequency or the magnetic field off resonance which would compromise the reproducibility of the operation of the state selector.

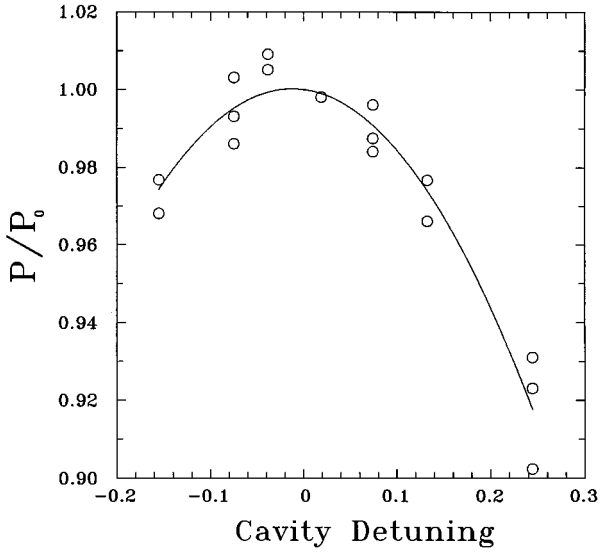

FIG. 9. The output power of the maser plotted as a function of the measured resonator detuning and arbitrarily normalized such that the peak amplitude of a fit of the data to Eq. (15) is set to 1. We infer from this fit that there is an offset $\Delta_0 = -0.014(30)$ in the measurement of the absolute resonator detuning. The estimate of this offset is refined using the data shown in Fig. 11.

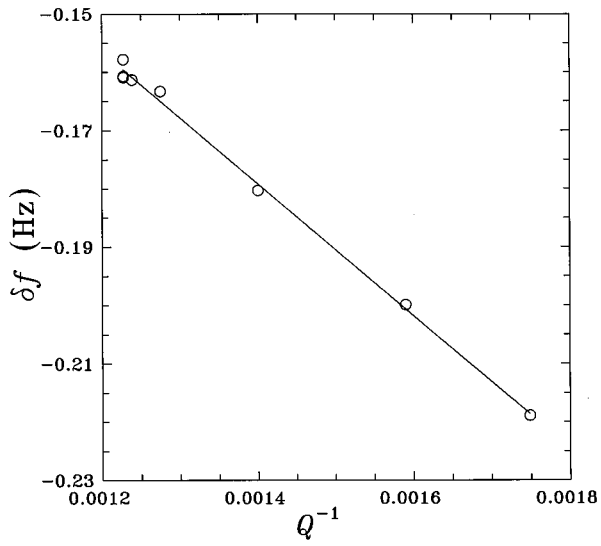

FIG. 10. The deviation δf of the maser oscillation frequency from the density-independent frequency f_0 plotted as a function of the inverse quality factor of the 1420-MHz resonator near zero detuning. A least squares fit of the data to a straight line extrapolates to a residual frequency shift of -20.7 ± 3.6 mHz at $Q^{-1} = 0$. The absolute tuning of the resonator is established by repeating this measurement as a function of the H-atom density (see Fig. 11).

A. Density-independent frequency ω_0 and the absolute resonator tuning

Our analysis commences with the establishment of the density-independent oscillation frequency ω_0 and the absolute resonator detuning. In Fig. 8 we plot the frequency of a FID response to a rf tipping pulse as a function of the H-atom density within the maser storage bulb. Referred to our reference oscillator, the data extrapolates to a zero-density frequency $f_0 = 1420.405\,783\,434(1)$ MHz where the uncertainty is a measure of the precision of the measurement. The actual value of $f_0 = \omega_0/2\pi$ as measured against a calibrated Rb frequency standard is several Hz lower.[20] We have not corrected the data for this offset since we are interested only in deviations of the maser oscillation frequency from this value.

As described previously, phase information from the FID's provides us with an accurate measure of the *relative* tuning of the split-ring resonator. It is essential to also have an accurate measure of the *absolute* resonator detuning. That is, we assume that standing waves in the microwave circuit external to the cavity may cause the *apparent* detuning of the resonator to be shifted by an offset Δ_0 from the *actual* detuning (i.e., that seen by the H atoms). We have employed two independent methods of determining the absolute resonator detuning. In Fig. 9, the normalized power output P/P_0 of the maser is plotted as a function of the resonator detuning determined from reflection measurements. The solid curve represents a least squares fit of the data to a quadratic of the form

$$\frac{P}{P_0} = 1 - \alpha(\Delta - \Delta_0)^2 \tag{15}$$

with α and Δ_0 as free parameters. We infer from the results of the fit that the absolute zero of the resonator detuning occurs at an apparent detuning $\Delta_0 = -0.014(30)$.

The second determination of the absolute resonator tuning is based upon an analysis of the maser frequency shift data taken at constant detuning near $\Delta = 0$. Equation (10) implies that the oscillation frequency of the maser should depend linearly on β or Q^{-1} at constant n_{H} and constant detuning. In the limit of zero detuning (we ignore terms in Δ^2) the residual frequency shift extrapolated to infinite Q is expected to be

$$\lim_{Q\to\infty} (\omega - \omega_0)|_{\Delta\approx 0} = (\Delta - \Delta_0)\Gamma_0 + (\Delta - \Delta_0 - \Omega)\Gamma_c\,, \tag{16}$$

where again the possibility of an apparent shift Δ_0 in the measurement of the detuning has been explicitly included. In Fig. 10 we plot an example of the deviation δf of the maser oscillation frequency from the density-independent frequency f_0 as a function of Q^{-1}. A least squares fit of the data to a straight line extrapolates to a residual frequency shift of -20.7 ± 3.6 mHz at $Q^{-1} = 0$. In Fig. 11 this residual shift is plotted as a function the H-atom density within the storage bulb. The residual has no obvious dependence on the H-atom density; nor would we expect there to be a detectable variation based upon either the calculations of Verhaar *et al.* or the measurements of Γ_0, Γ_c, and Ω presented later. We attribute the average residual frequency shift of $-0.021(4)$

[20]Note that even after this correction has been applied, f_0 is higher than the unperturbed zero field hyperfine frequency of the H atom. This is due to a combination of density-independent shifts caused by the bias magnetic field, collisions between H atoms and the ^{4}He buffer gas, and collisions of H atoms with the walls of the storage bulb.

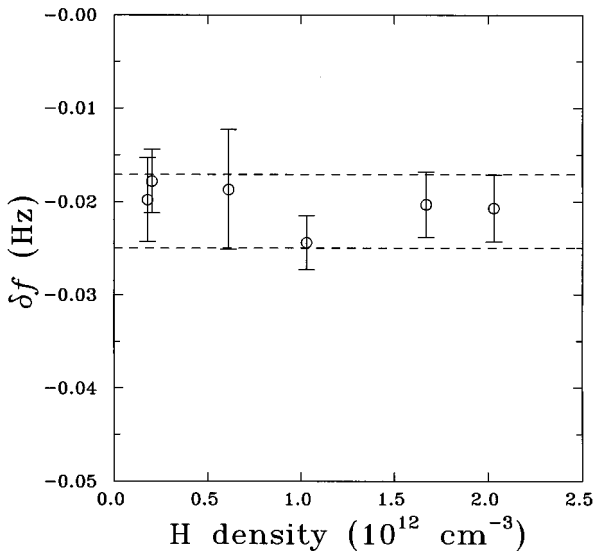

FIG. 11. Compilation of the residual frequency shifts extrapolated to infinite Q near zero detuning (see Fig. 10) shown as a function of the H-atom density within the maser storage bulb. The average residual frequency shift of $-0.021(4)$ Hz (indicated by the dashed lines) is independent of the H-atom density as expected, and is attributed to an offset $\Delta_0=-0.046(1)$ between the measured and actual detuning of the resonator. Further references to Δ have been corrected for this offset.

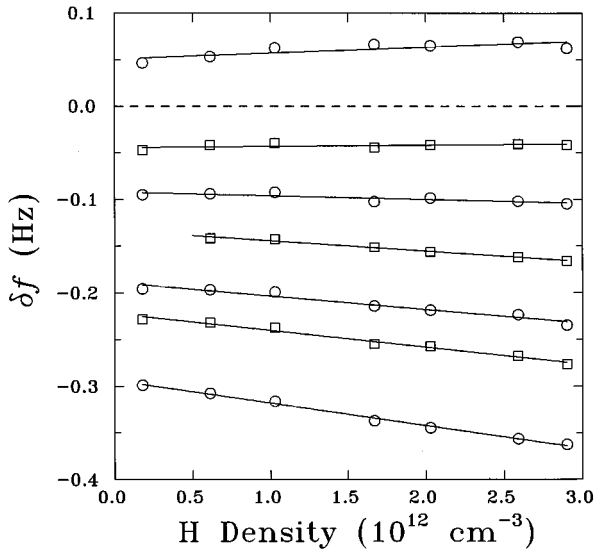

FIG. 12. The deviation of the maser oscillation frequency from ω_0 measured at constant Q and plotted as a function of the H-atom density in the storage bulb for a number of resonator detunings ranging from $\Delta\approx-0.2$ (lowest data set) to $\Delta\approx0.2$ (uppermost data set). The straight lines represent least squares fits to the data. Near $\Delta=0.09$ (second data set from the top) the slope of the fit to the data passes through zero. In the "classical" interpretation of spin-exchange collisions this *would* correspond to the spin-exchange tuning point $\Delta=\Delta'$ *except* for the fact that the maser oscillation frequency is offset from zero. We interpret this offset as being due to hyperfine interactions between colliding atoms.

Hz as being due solely to an offset of the resonator tuning from zero [i.e., $(\Delta-\Delta_0)\Gamma_0$, where $\Delta\approx0$ is the measured detuning at which the data were taken]. In the following section we obtain a measurement of Γ_0 which to first order is independent of the absolute resonator tuning and thus we are able to determine that $\Delta_0=-0.046(10)$. This result is consistent with the previous determination of Δ_0; it is the value we adopt throughout the remainder of this analysis. From this point on, the detunings which are reported have been corrected for this apparent shift.

B. $\bar{\lambda}_0$, Γ_0 and the classical spin-exchange tuning criterion

In Fig. 12 we plot the deviation of the maser oscillation frequency from ω_0 as a function of the H-atom density in the storage bulb for several detunings of the split-ring resonator at constant Q. The lowest data set corresponds to a detuning $\Delta\approx-0.2$ while the uppermost data set was taken at $\Delta\approx0.2$. Each data set has been fit to a straight line to indicate the average slope over the full range of densities. There is an obvious change in the slope of the data from negative to positive as the detuning is increased. Close to $\Delta\approx0.09$ (the data set second from the top) the average *slope* of the data passes through zero. In the traditional interpretation of spin-exchange collisions [c.f. Eq. (12)], this corresponds to the spin-exchange tuning condition $\Delta=\Delta'$. We note, however, that the residual frequency shift at this point is *not* zero as predicted by Eqs. (10) and (12) with $\Omega=0$.

Based upon the full VKSLC theory, one expects the frequency shift at constant detuning and Q to be linear in n_{H} except for any deviations induced by changes in the population of the $m_F=0$ hyperfine states. In general the dependence of $(\rho_{cc}+\rho_{aa})$ on n_{H} is a complicated function of the maser dynamics. Given the present experimental design, it was not possible to measure the relative populations of the hyperfine states; we therefore make no attempt to untangle the dependence of the frequency shift on $(\rho_{cc}+\rho_{aa})$. We do, however, implicitly rely on a prediction of the computer simulation of the maser dynamics. That is, we assume that variations in $(\rho_{cc}+\rho_{aa})$ across the operating range of the maser are indeed small and that we can adequately model the frequency shift by fitting each data set in Fig. 12 to a straight line. This topic is discussed further in the following section.

Using the assumption made above we extrapolate the frequency shifts at constant Q and Δ to zero density. From Eq. (10) we expect that this extrapolated shift is given by

$$\lim_{n_{\mathrm{H}}\to0}(\omega-\omega_0)=[\Delta+\beta\bar{\lambda}_0(1+\Delta^2)]\Gamma_0. \tag{17}$$

Obviously the maser does not oscillate under these conditions; however, by fitting our data to Eq. (17) we are able to determine both Γ_0 and $\bar{\lambda}_0$. In fact, since the extrapolation procedure is independent of the density enhancement factor κ, the results we obtain for these two parameters are independent of the computer simulation results.

The extrapolated zero-density frequency shifts obtained from the data in Fig. 12 are plotted in Fig. 13 along with a least squares fit to Eq. (17). Even though it is slight, the curvature in the fit to the data is significant and indicates that $\bar{\lambda}_0$ is negative. The linear term in the fit to Eq. (17) depends only upon the relative measurement of Δ to first order and thus provides a reliable measurement of the density-independent broadening. We find $\Gamma_0=5.47(11)$ s^{-1}; the

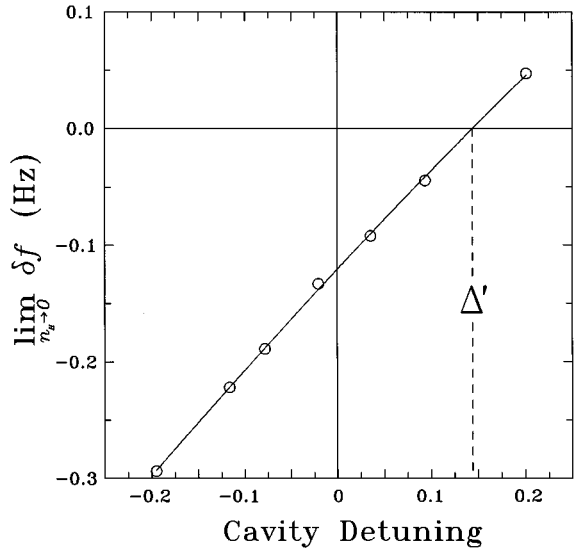

FIG. 13. The extrapolated zero density shift of the maser oscillation frequency measured at constant Q (from Fig. 12) plotted as a function of the absolute resonator detuning. Uncertainties are smaller than the symbols used to represent the data. The negative curvature exhibited by the fit of the data to Eq. (17), which is quadratic in Δ is significant and indicates that $\bar{\lambda}_0$ is negative at the experimental temperature of 0.5 K. The parameters Γ_0 and $\bar{\lambda}_0$ are determined from this fit. The result $\Gamma_0 = 5.47(11)\ \mathrm{s}^{-1}$ is independent of the absolute resonator detuning to first order, and when combined with the residual frequency shift described in Fig. 11 provides a means of determining the absolute resonator detuning. We find $\bar{\lambda}_0 = -21.7(2.8)\ \text{Å}^2$ where the number in parentheses represents all sources of experimental uncertainty. The detuning at which the extrapolated zero density frequency shift is zero corresponds to the detuning Δ' which in the DIS interpretation of spin-exchange *should* make the maser oscillation frequency independent of n_{H}.

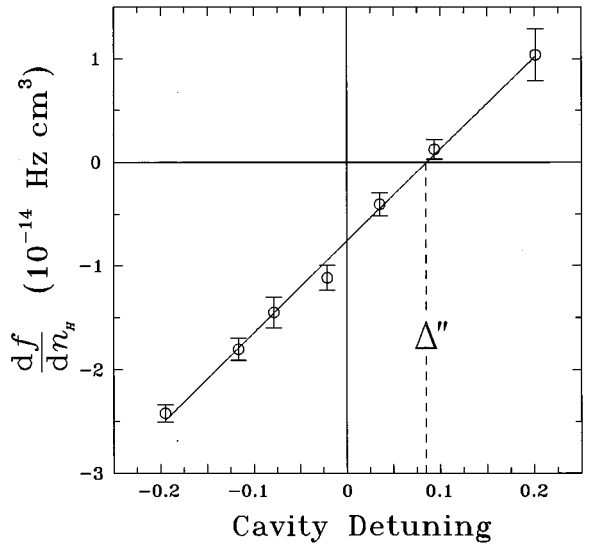

FIG. 14. The rate of change of the maser oscillation frequency with respect to the H-atom density at constant Q plotted as a function of the absolute resonator detuning. The slope of the straight line which has been fitted to the data is related to the density-dependent broadening rate Γ_c from which we obtain the result $\bar{\sigma}_1(\rho_{cc}+\rho_{aa})+\bar{\sigma}_2 = 0.385(30)\ \text{Å}^2$. The detuning for which the fit to the data passes through zero corresponds to the modified spin-exchange tuning point Δ'' described in the text. The difference between Δ'' and Δ' (see Fig. 13) gives an accurate measurement of the h-i induced frequency shift parameter Ω.

value used in the previous section to establish the absolute tuning of the 1420 MHz resonator. The ratio of the linear term to the constant term in the fit to Eq. (17) provides a measure of the product $\beta\bar{\lambda}_0$. β is accurately known from measurements of the filling factor [34] and the quality factor and thus the largest uncertainty in our result for the classical[21] spin-exchange frequency shift cross section $\bar{\lambda}_0$, is due to the uncertainty in the absolute detuning of the resonator. We find $\bar{\lambda}_0 = -21.7(2.8)\ \text{Å}^2$ [38].

Before leaving this topic, it is worth pointing out that the detuning at which the extrapolated zero-density frequency shift passes through zero corresponds to the detuning Δ' which in the DIS interpretation of spin-exchange *should* make the maser oscillation frequency independent of n_{H}. From the data shown in Fig. 13 we infer that $\Delta' = 0.144(3)$. In the following section it will be seen that the offset of the oscillation frequency from ω_0 *does* depend on n_{H} when $\Delta = \Delta'$.

[21]We use the term "classical spin-exchange frequency shift cross section" for $\bar{\lambda}_0$ as it corresponds to the single frequency-shift cross section in the DIS approximation.

C. $\bar{\sigma}_1(\rho_{cc}+\rho_{aa})+\bar{\sigma}_2$, Ω, and the modified spin-exchange tuning criterion

The average rate of change of the maser oscillation frequency shift with respect to the H-atom density is obtained from the slope of the fits to the data shown in Fig. 12 and is plotted as a function of the absolute resonator detuning in Fig. 14. Neglecting any dependence of $(\rho_{cc}+\rho_{aa})$ on n_{H}, Eq. (10) implies that

$$\frac{\partial}{\partial n_{\mathrm{H}}}(\omega-\omega_0) = \bar{v}[\Delta+\beta\bar{\lambda}_0(1+\Delta^2)-\Omega] \times[\bar{\sigma}_1(\rho_{cc}+\rho_{aa})+\bar{\sigma}_2]. \tag{18}$$

While the dependence of $\partial(f-f_0)/\partial n_{\mathrm{H}}$ is expected to be quadratic in Δ, the uncertainties in the data are too large to justify fitting to more than a straight line, as indicated in Fig. 14. Keeping in mind that we have plotted the *average* rate of change of the maser oscillation frequency with respect to n_{H}, we interpret the detuning for which the fit to the data passes through zero as a measure of the modified spin-exchange tuning criterion $\Delta = \Delta''$. We infer from Fig. 14 that $\Delta'' = 0.085^{+0.006}_{-0.018}$.

By examining Eq. (10), one finds that to first approximation the h-i frequency shift parameter [Eq. (11)] is given by the difference $\Delta''-\Delta'$ between the two spin-exchange tuning criteria. More precisely, Ω is equal to

$$\Omega = (\Delta''-\Delta')\left[\frac{(1-\Delta'\Delta'')}{(1+\Delta'^2)}\right], \tag{19}$$

which for small detunings reduces to $\Delta''-\Delta'$. The importance of writing Ω in this fashion is that it is readily seen that Ω can be accurately determined essentially independent of the absolute resonator tuning and the H-atom density calibration. From the zero crossings indicated in Figs. 13 and 14 we obtain a value $\Omega=-0.057(+0.009/-0.021)$ for the *h-i* frequency shift parameter. This result has been reported previously [37].

Neglecting terms in Δ^2, the slope of the fit to the data shown in Fig. 14 is given by

$$\frac{\partial}{\partial\Delta}\left(\frac{\partial}{\partial n_{\mathrm{H}}}(\omega-\omega_0)\right)\Bigg|_{\Delta\approx 0}=\bar{v}[\bar{\sigma}_1(\rho_{cc}+\rho_{aa})+\bar{\sigma}_2], \quad (20)$$

allowing us to obtain a direct measurement of the spin-exchange-induced broadening. We infer from Fig. 14 that $\bar{\sigma}_1(\rho_{cc}+\rho_{aa})+\bar{\sigma}_2=0.385(30)$ Å^2, a result which, while it depends upon the absolute calibration of the H-atom density inside the oscillating maser, depends only upon a relative measurement of Δ. The uncertainty in the density enhancement factor κ (about 5%) is reflected in the uncertainty which is reported for $\bar{\sigma}_1(\rho_{cc}+\rho_{aa})+\bar{\sigma}_2$. Combining this result with the determination of Ω, we infer that $\bar{\lambda}_1(\rho_{cc}+\rho_{aa})+\bar{\lambda}_2=-0.022^{+0.005}_{-0.010}$ Å^2.

VI. CONCLUDING REMARKS

We have described the measurement of a number of spin-exchange parameters relevant to the operation of hydrogen masers at temperatures below 1 K. Specifically, in terms of the fully quantum mechanical theory of hydrogen spin-exchange collisions developed by VKSLC [12,13], we have measured the classical spin-exchange frequency shift cross section $\bar{\lambda}_0$, the hyperfine-induced (*h-i*) spin-exchange frequency shift parameter Ω, and the combined spin-exchange broadening cross section $\bar{\sigma}_1(\rho_{cc}+\rho_{aa})+\bar{\sigma}_2$. From these results we infer a value for the combined spin-exchange frequency shift cross section $\bar{\lambda}_1(\rho_{cc}+\rho_{aa})+\bar{\lambda}_2$. In each case, measurements were carried out at a temperature of 0.5 K and with half of the colliding atoms in the $m_F=0$ states [i.e., $(\rho_{cc}+\rho_{aa})=0.5$].

The most significant result of this work is the measurement of a nonzero value for the *h-i* spin-exchange cross section. Our data is clearly inconsistent with a conventional DIS treatment of the hydrogen atom spin-exchange problem which predicts that Ω should be identically equal to zero. The data thus highlights the importance of including hyperfine interactions in the analysis of spin-exchange collisions at low temperatures.

The principle systematic uncertainty in the interpretation of our data is the fact that we must rely on a computer simulation of the quasistatic dynamics of the maser to determine the absolute H-atom density within the storage bulb of the *oscillating* maser. Less uncertain, but nevertheless a concern, is our determination of the *absolute* tuning of the 1420-MHz resonator. Care has been taken to ensure that the value we report for Ω is independent of both of these sources of potential systematic errors. Consequently, the principle systematic uncertainty in our measurement of Ω arises from our determination of *relative* resonator tunings. We have, however, demonstrated that this can be done with considerable accuracy using information contained in a free-induction-decay response to a magnetic resonance tipping pulse.

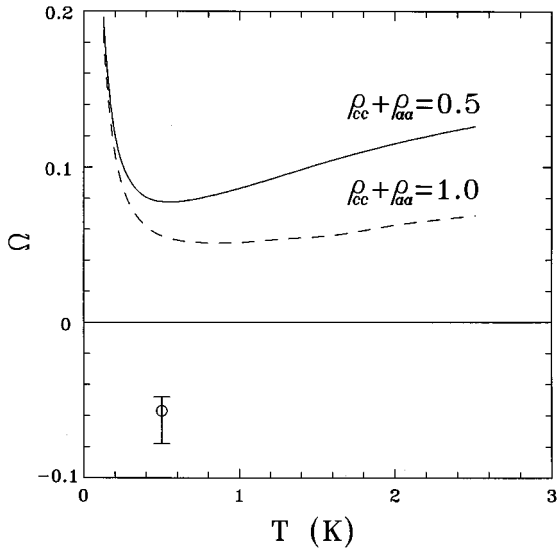

FIG. 15. A plot of the dimensionless hyperfine induced frequency shift parameter Ω at low temperatures as calculated by VKSLC [12,13,20]. The solid curve corresponds to $(\rho_{cc}+\rho_{aa})=0.5$ and is therefore the result to be compared to our experimental value (open circle). The other case corresponding to $(\rho_{cc}+\rho_{aa})=1$ (dashed line) is included to illustrate the variation of Ω as the composition of the atomic gas is changed in terms of the hyperfine level populations.

The value we report for the classical spin-exchange frequency shift cross section $\bar{\lambda}_0$ depends upon the absolute resonator tuning, but not upon the computer simulation. This tuning is determined in a swept frequency cavity reflection measurement and, as such, is susceptible to systematic errors introduced by standing waves in the microwave circuitry external to the 1420-MHz resonator. We have used two independent techniques to measure the perturbing influence of standing waves, and thus believe that we have properly accounted for this effect in our analysis of the data.

The least certain result we present[22] is the value for the combined spin-exchange broadening cross section $\bar{\sigma}_1(\rho_{cc}+\rho_{aa})+\bar{\sigma}_2$. This result depends upon our determination of the atomic density within the storage bulb of the oscillating maser. We have been forced to use a computer simulation to infer this density from measurements made under non-oscillating conditions. We do, however, have reason to believe that the simulation gives a reasonably accurate picture of the maser dynamics [8,9]. Furthermore, recent accurate measurements of the longitudinal spin-exchange relaxation rate for a gas of atomic hydrogen at 1 K [26] can be used to estimate the broadening cross section measured in this experiment. As described below, this comparison lends further support to the value we report here.

Comparison of our experimental results with the theoretical predictions of VKSLC made using ''state-of-the-art'' in-

[22]The result for the combined spin-exchange frequency shift cross section $\bar{\lambda}_1(\rho_{cc}+\rho_{aa})+\bar{\lambda}_2$ is inferred from Ω and $\bar{\sigma}_1(\rho_{cc}+\rho_{aa})+\bar{\sigma}_2$ and is thus susceptible to the same uncertainties.

teratomic potentials leaves several questions to be answered. While there is qualitative agreement between theory and experiment as far as the magnitude of the various quantities is concerned, a number of serious quantitative disagreements exist. Most significant perhaps is the fact that the value we measure for the *h-i* shift cross section $\Omega = -0.057^{+0.009}_{-0.021}$ has the opposite sign from the theoretically predicted value $\Omega = 0.078$ [20] at 0.5 K with $(\rho_{cc} + \rho_{aa}) = 0.5$. Note that with reference to Figs. 13 and 14, the theoretical prediction suggests that Δ'' (Fig. 14) should occur at a lower detuning than Δ' (Fig. 13) rather than at a higher detuning. Our result for Ω has been plotted in Fig. 15 along with the predictions of VKSLC for selected values of $(\rho_{cc} + \rho_{aa})$. Efforts to reconcile this discrepancy by careful examination of the theoretical calculations have not been successful [20]. Furthermore, no reasonable variation of the known potentials has yet been shown to produce the necessary change in sign required to bring the two results into agreement.[23]

One must ask whether the effect we observe is indeed caused by hyperfine interactions between colliding H atoms, or whether it is the sum of that effect and some other frequency shift for which we have not yet accounted. One such shift which has plagued similar measurements in the past is due to collisions between radiating atoms and either $|b\rangle$ or $|d\rangle$ state atoms which are also present in the storage bulb. When these collisions occur in the presence of magnetic field gradients they can give rise to a frequency shift known as a *magnetic inhomogeneity shift* [40]. This effect, however, is completely suppressed by the application of magnetic fields much weaker than those used in the present work. It is difficult to imagine other mechanisms which could have produced the discrepancy we observed.

Walsworth and co-workers [41] have reported an experiment in which an adiabatic fast passage technique was used to look for indications of the *h-i* frequency shift in a conventional *room-temperature maser*. The quantity which was measured in their experiment corresponds to the difference in Ω between two conditions in which the distribution of atoms between the various hyperfine states was changed. The results of their experiment are in accord with the work we report here, in that the observed effect also had the opposite sign to that predicted by VKSLC.

A significant quantitative disagreement between theory and experiment also exists in the case of the classical spin-exchange frequency shift $\overline{\lambda}_0$. The value we report, $\overline{\lambda}_0 = -21.7(2.8)$ Å^2, is nearly twice as large as the theoretical prediction $\overline{\lambda}_0 = -11.8$ Å^2 at 0.5 K [20]. This is in marked contrast to the situation over the temperature range 77–363 K, where satisfactory agreement between theory and experiment is obtained [42,43]. Our results, and those of a few previous workers, are compared with several theoretical calculations of $\overline{\lambda}_0$ in Fig. 16.[24] Note that the difference between the DIS and fully quantum mechanical predictions are negligible on this scale. The discrepancies between the various theoretical predictions are due solely to differences in the potentials used in the calculations. Given the sensitivity of $\overline{\lambda}_0$ to the interatomic potentials and the fact that it is expected to be insensitive to the influence of hyperfine interactions during collisions, our measurement of $\overline{\lambda}_0$ may prove to be an excellent parameter against which to gauge future modifications to the H-H interatomic potentials.

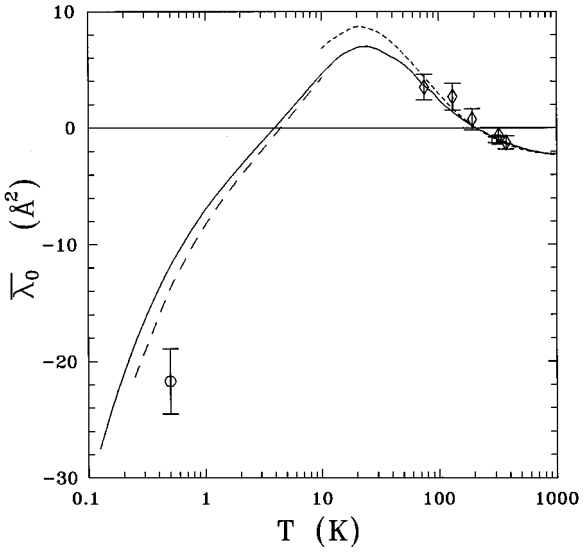

FIG. 16. A comparison of experimental and theoretical results for the classical spin-exchange frequency shift cross section $\overline{\lambda}_0$. The solid line represents the calculations of VKSLC and is expected to be the most accurate. Also shown are the earlier calculations of Allison [51] (short dashes) and Berlinsky and Shizgal [45] (long dashes). Deviations between the calculated results are due to the details of the interatomic potentials used by these authors; the difference between DIS and the fully quantum mechanical calculations of $\overline{\lambda}_0$ are negligible on this scale. Our result for $\overline{\lambda}_0$ (indicated by the open circle) deviates from the theoretical calculations in contrast to the situation at higher temperatures. Also shown in the figure are the measured values of $\overline{\lambda}_0$ reported by Crampton *et al.* [42] (open square) and Desaintfuscien *et al.* [43] (open diamonds).

Our final result, $\overline{\sigma}_1(\rho_{cc} + \rho_{aa}) + \overline{\sigma}_2 = 0.385(30)$ Å^2 for the combined spin-exchange broadening cross sections $\overline{\sigma}_1$ and $\overline{\sigma}_2$ with $(\rho_{cc} + \rho_{aa}) = 0.5$, is compared to theoretical calculations in Fig. 17. Also shown are a number of experimentally determined values for the broadening cross section at higher temperatures where $\overline{\sigma}_2$ is expected to dominate [44]. The agreement at high temperature is again significantly better than at low temperature where $\overline{\sigma}_1$ is expected to be the

[23]The H-H interatomic potentials are the most accurately known of all interatomic potentials. Improvements to the relevant potentials have been made [39] since the original calculations of VKSLC; however, these changes do not produce significant modifications to the values of the theoretical spin-exchange cross sections relevant to our work [20].

[24]The definitions of the spin-exchange frequency shift and broadening cross sections used by early authors differ from the notation introduced by VKSLC. When necessary, here and in Fig. 17, we have modified the reported cross sections to be consistent with VKSLC.

dominant term.[25] Unlike $\overline{\lambda_0}$, $\overline{\sigma}_1$ is sensitive to the inclusion of hyperfine interactions in the relevant calculations. The difference between the calculations of VKSLC (solid line) and the earlier calculation of Berlinsky and Shizgal [45] (dashed line) is thus due both to this effect and the fact that different potentials were used.

During a recent experiment intended as a means of checking the accuracy of the broadening cross section reported here, the longitudinal spin-relaxation rate $1/T_1$ for a gas of H atoms at 1.2 K was measured [26].[26] In the DIS approximation one finds that spin-exchange collisions between homonuclear species yields $T_1/T_2=\frac{1}{2}$, where T_2 is the transverse broadening cross section. Assuming this relationship remains valid at 1.2 K, we can infer a value for $\overline{\sigma}_1(\rho_{cc}+\rho_{aa})+\overline{\sigma}_2$.[27] The result so obtained has been plotted in Fig. 17 (open square). The consistent deviation of our experimental results for $\overline{\sigma}_1(\rho_{cc}+\rho_{aa})+\overline{\sigma}_2$ (obtained in independent measurements) from the curve predicted by VKSLC leads us to suspect that the cause of the discrepancy lies in the theoretical description of the spin-exchange problem.

The primary implications of the work reported in this paper are twofold. From a purely technological standpoint, the fact that our data exhibits qualitative agreement with the predictions of the fully quantum mechanical spin-exchange calculations of VKSLC implies that hyperfine interactions during spin-exchange collisions are likely to play an important role in the operation of low-temperature H masers. The detailed manner in which these effects will influence the stability of such masers is yet unclear given the apparent discrepancies between theory and experiment. Effects analogous to those studied here may limit the ultimate frequency stability of other devices such as atomic fountain clocks [48–50], and hence the importance of resolving these discrepancies extends beyond the design of future cryogenic hydrogen masers. From a more fundamental point of view, the disagreement between our data and the predictions of VKSLC lead us to conclude that spin-exchange collisions between H atoms at low temperatures are not fully understood. Either some as yet unknown effect is missing from the current description of the operation of H masers at low temperatures, or the details of the H-H interatomic potentials used to calculate the spin-exchange cross sections are inadequate. The latter possibility is intriguing as some of the parameters we have measured are quite sensitive to the very-long-range part of the interatomic potentials. They may well prove to be valuable indexes against which future refinements of the potentials are gauged.

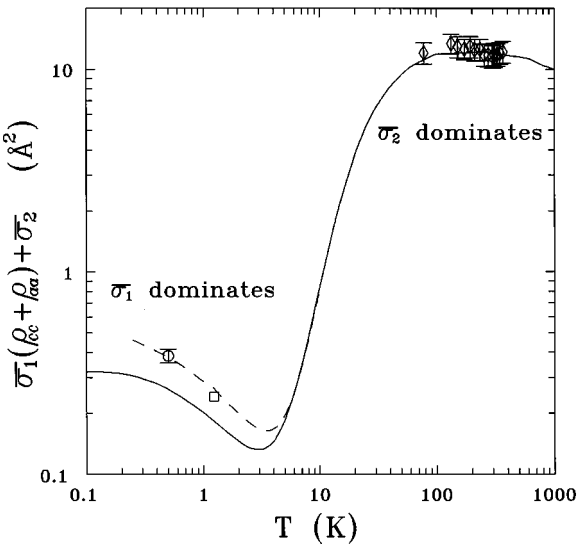

FIG. 17. A comparison of experimental and theoretical results for the combined spin-exchange broadening cross section $\overline{\sigma}_1(\rho_{cc}+\rho_{aa})+\overline{\sigma}_2$ for $(\rho_{cc}+\rho_{aa})=0.5$. The solid curve represents the calculations of VKSLC and is expected to be the most accurate. At high temperatures $\overline{\sigma}_2$ dominates and the broadening is expected to be independent of $(\rho_{cc}+\rho_{aa})$. At low temperatures $\overline{\sigma}_1$ is expected to dominate. Similar to the situation for $\overline{\lambda_0}$, agreement between theory and experiment is better at high temperature than at lower temperature. The value we report here is represented by the open circle. The other low-temperature point (open square) has been inferred from a recent experiment carried out to verify our result at 0.5 K [26]. Also shown are the high-temperature experimental results of Desaintfuscien and Audoin [44] (open diamonds). The earlier calculations of Berlinsky and Shizgal [45] (dashed curve) which neglect hyperfine interactions are shown for comparison. The calculations of Allison [51] at high temperatures are not readily distinguished from those of VKSLC and so we have not included them in this figure.

ACKNOWLEDGMENTS

This work was supported by the Natural Sciences and Engineering Research Council (NSERC) of Canada. The authors are particularly grateful to S. B. Crampton and B. J. Verhaar, with whom they have shared many useful and enlightening discussions regarding the UBC CHM program, and to A. J. Berlinsky and R. W. Cline, who made essential contributions to the early stages of the program. The early part of the program also benefited from a U.S. National Bureau of Standards Precision Measurement Grant. Finally, we are indebted to the UBC mechanical and electronics shops for their excellent support.

[25]If we assume that $\overline{\sigma}_1 \gg \overline{\sigma}_2$ at 0.5 K as predicted by VKSLC, our measurements imply that $\overline{\sigma}_1=0.77(6)$ Å^2.

[26]Specifically, the rate at which the difference between the occupation of the $|a\rangle$ and $|c\rangle$ states returns to its thermal equilibrium value following a π tipping pulse was studied. This type of measurement was originally performed by Morrow *et al.* [30,24,46]; however, systematic uncertainties regarding the determination of the filling factor [31] in these early experiments led us to question the accuracy of their results. In the experiment reported in Ref. [26] we have taken great care to establish an accurate calibration of the H-atom density and to account for recombination during the measurement.

[27]Stoof *et al.* [47] have calculated the spin-exchange relaxation rates which influence the diagonal elements of the density matrix. Comparison of these results with those of VKSLC for the relevant off diagonal elements leads one to conclude that this relationship should hold to within 5% at 1.2 K. While no direct experimental evidence for this relationship exists at these low temperatures, it has been demonstrated that an analogous relationship for spin-exchange collisions between heteronuclear species holds true in the case of hydrogen-deuterium collisions at 1 K [31].

[1] R. F. C. Vessot, M. W. Levine, and E. M. Mattison, *Proceedings of the Ninth Annual Precise Time and Time Interval (PTTI) Applications and Planning Meeting*, NASA Technical Memorandum No. 78104 (NASA, Gaithersburg, MD, 1978), p. 549.
[2] S. B. Crampton, W. D. Phillips, and D. Kleppner, Bull. Am. Phys. Soc. **23**, 86 (1978).
[3] W. N. Hardy and M. Morrow, J. Phys. (Paris) Colloq. **42**, C8-171 (1981).
[4] A. J. Berlinsky and W. N. Hardy, in *Proceedings of the Thirteenth Annual Precise Time and Time Interval (PTTI) Applications and Planning Meeting*, NASA Conference Publ. No. 2220 (NASA, Gaithersburg, MD, 1982), p. 547.
[5] H. F. Hess, G. P. Kochanski, J. M. Doyle, T. J. Greytak, and D. Kleppner, Phys. Rev. A **34**, 1602 (1986).
[6] M. D. Hürlimann, W. N. Hardy, A. J. Berlinsky, and R. W. Cline, Phys. Rev. A **34**, 1605 (1986).
[7] R. L. Walsworth, I. F. Silvera, H. P. Godfried, C. C. Agosta, R. F. C. Vessot, and E. M. Mattison, Phys. Rev. A **34**, 2550 (1986).
[8] M. D. Hürlimann, W. N. Hardy, M. E. Hayden, and R. W. Cline, in *Frequency Standards and Metrology*, edited by A. De Marchi (Springer-Verlag, Berlin, 1989), p. 95.
[9] M. D. Hürlimann, Ph.D. thesis, University of British Columbia, 1989.
[10] J. Vanier and C. Audouin, *The Quantum Physics of Atomic Frequency Standards* (Higler, Bristol, 1989).
[11] W. N. Hardy, M. D. Hürlimann, and R. W. Cline, Jpn. J. Appl. Phys. **26**, 2065 (1987).
[12] B. J. Verhaar, J. M. V. A. Koelman, H. T. C. Stoof, O. J. T. Luiten, and S. B. Crampton, Phys. Rev. A **35**, 3825 (1987).
[13] J. M. V. A. Koelman, S. B. Crampton, H. T. C. Stoof, O. J. T. Luiten, and B. J. Verhaar, Phys. Rev. A **38**, 3535 (1988).
[14] J. M. V. A. Koelman, S. B. Crampton, H. T. C. Stoof, O. J. Luiten, and B. J. Verhaar, in *Spin Polarized Quantum Systems*, edited by S. Stringari (World Scientific, Singapore, 1989), p. 223.
[15] S. B. Crampton, Phys. Rev. **158**, 57 (1967).
[16] P. L. Bender, Phys. Rev. **132**, 2154 (1963).
[17] L. C. Balling, R. J. Hanson, and F. M. Pipkin, Phys. Rev. **133**, A607 (1964).
[18] S. B. Crampton, Ph.D. thesis, Harvard University, 1964.
[19] S. B. Crampton and H. T. M. Wang, Phys. Rev. A **12**, 1305 (1975).
[20] B. J. Verhaar (private communication).
[21] Martin D. Hürlimann, A. John Berlinsky, Richard W. Cline, and Walter N. Hardy, IEEE Trans. Instrum. Measurement IM-**36**, 584 (1987).
[22] M. E. Hayden, Ph.D. thesis, University of British Columbia, 1991.
[23] P. J. Nacher, M. Cornut, and M. E. Hayden, J. Low Temp. Phys. **97**, 416 (1994).
[24] W. N. Hardy, M. Morrow, R. Jochemsen, and A. J. Berlinsky, Physica **109&110B**, 1964 (1982).
[25] M. Morrow, R. Jochemsen, A. J. Berlinsky, and W. N. Hardy, Phys. Rev. Lett. **46**, 195 (1981); **47**, 455(E) (1981).
[26] M. E. Hayden and W. N. Hardy, Phys. Rev. Lett. (to be published).
[27] The dilution unit, comprising a still, continuous heat exchanger, and mixing chamber has a semicircular cross section rather than the usual circular one in order to leave ample room for waveguide, coax, tuning rods, etc. It was developed by R. W. Cline.
[28] K. E. Kürten and M. L. Ristig, Phys. Rev. B **31**, 1346 (1985).
[29] W. N. Hardy and L. A. Whitehead, Rev. Sci. Instrum. **52**, 213 (1981).
[30] W. N. Hardy, M. Morrow, R. Jochemsen, B. W. Statt, P. R. Kubik, R. M. Marsolais, A. J. Berlinsky, and A. Landesman, Phys. Rev. Lett. **45**, 453 (1980).
[31] M. E. Hayden and W. N. Hardy, J. Low Temp. Phys. **99**, 787 (1995).
[32] D. R. Williams, W. Lum, and S. Weinreb, Microw. J. **23**, 73 (1980).
[33] M. R. Morrow, Ph.D. thesis, University of British Columbia, 1983.
[34] M. E. Hayden and W. N. Hardy, Rev. Sci. Instrum. (to be published).
[35] S. Bloom, J. Appl. Phys. **28**, 800 (1957).
[36] Discussed in most texts on microwave electronics. See, for example, Robert E. Collin, *Foundations for Microwave Engineering* (McGraw-Hill, Toronto, 1966).
[37] Michael E. Hayden, Martin D. Hürlimann, and Walter N. Hardy, IEEE Trans. Instrum. Measurement **42**, 314 (1993).
[38] M. E. Hayden, M. D. Hürlimann, and W. N. Hardy, in *Proceedings, IEEE International Frequency Control Symposium* (Institute of Electrical and Electronics Engineers, Piscataway, NJ, 1994), p. 670.
[39] L. Wolniewicz, J. Chem. Phys. **99**, 1851 (1993).
[40] S. B. Crampton and H. T. M. Wang, in *Proceedings of the 28th Annual Symposium on Frequency Control* (Electronics Industries Association, Washington, 1974), p. 355.
[41] Ronald L. Walsworth, Isaac F. Silvera, Edward M. Mattison, and Robert C. Vessot, Phys. Rev. A **46**, 2495 (1992).
[42] S. B. Crampton, J. A. Duvivier, G. S. Read, and E. R. Williams, Phys. Rev. A **5**, 1752 (1972).
[43] M. Desaintfuscien, J. Viennet, C. Audouin, and J. Vanier, J. Phys. Lett. (Paris) **36**, 281 (1975).
[44] M. Desaintfuscien and C. Audoin, Phys. Rev. A **13**, 2070 (1976).
[45] A. J. Berlinsky and B. Shizgal, Can. J. Phys. **58**, 881 (1980).
[46] M. Morrow and W. N. Hardy, Can. J. Phys. **61**, 956 (1983).
[47] H. T. C. Stoof, J. M. V. A. Koelman, and B. J. Verhaar, Phys. Rev. B **38**, 4688 (1988).
[48] E. Tiesinga, S. J. M. Kuppens, B. J. Verhaar, and H. T. C. Stoof, Phys. Rev. A **43**, 5188 (1991).
[49] E. Tiesinga, B. J. Verhaar, H. T. C. Stoof, and D. van Bragt, Phys. Rev. A **45**, R2671 (1992).
[50] Kurt Gibble and Steven Chu, Phys. Rev. Lett. **70**, 1771 (1993).
[51] A. C. Allison, Phys. Rev. A **5**, 2695 (1972).